EXHIBIT 3

SCIENCE TRANSLATIONAL MEDICINE | RESEARCH ARTICLE

EPILEPSY

Filamin A inhibition reduces seizure activity in a mouse model of focal cortical malformations

Longbo Zhang[1,2], Tianxiang Huang[1,2], Shannon Teaw[1], Lena H. Nguyen[1], Lawrence S. Hsieh[1], Xuan Gong[1,2], Lindsay H. Burns[3], Angélique Bordey[1]*

Epilepsy treatments for patients with mechanistic target of rapamycin (mTOR) disorders, such as tuberous sclerosis complex (TSC) or focal cortical dysplasia type II (FCDII), are urgently needed. In these patients, the presence of focal cortical malformations is associated with the occurrence of lifelong epilepsy, leading to severe neurological comorbidities. Here, we show that the expression of the actin cross-linking protein filamin A (FLNA) is increased in resected cortical tissue that is responsible for seizures in patients with FCDII and in mice modeling TSC and FCDII with mutations in phosphoinositide 3-kinase (PI3K)–ras homolog enriched in brain (Rheb) pathway genes. Normalizing FLNA expression in these mice through genetic knockdown limited cell misplacement and neuronal dysmorphogenesis, two hallmarks of focal cortical malformations. In addition, *Flna* knockdown reduced seizure frequency independently of mTOR signaling. Treating mice with a small molecule targeting FLNA, PTI-125, before the onset of seizures alleviated neuronal abnormalities and reduced seizure frequency compared to vehicle-treated mice. In addition, the treatment was also effective when injected after seizure onset in juvenile and adult mice. These data suggest that targeting FLNA with either short hairpin RNAs or the small molecule PTI-125 might be effective in reducing seizures in patients with TSC and FCDII bearing mutations in PI3K-Rheb pathway genes.

INTRODUCTION

Focal cortical dysplasia type II (FCDII) and tuberous sclerosis complex (TSC) are neurodevelopmental disorders caused by mutations in the phosphoinositide 3-kinase (PI3K)–AKT–mechanistic target of rapamycin (mTOR) pathway genes, leading to mTOR hyperactivity, focal malformations of the developing cortex, and seizures in 80 to 90% of the patients (*1*, *2*). Nearly two-thirds of these patients are refractory to treatment with antiepileptic drugs and experience lifelong seizures, leading to a spectrum of neurocognitive and psychological disabilities (*3*). The current treatments are surgical resection of the focal cortical malformations (FCMs) and administration of antiepileptic drugs, including in TSC, everolimus, a rapamycin analog that inhibits mTOR activity. These treatments either are invasive or are associated with serious adverse events, and neither is fully effective (*4*). There is thus a critical need to improve epilepsy treatment in patients with TSC and FCDII.

One strategy to develop better treatments is to identify molecules that contribute to the formation of cortical malformations. With this goal in mind, we recently determined that the actin cross-linking and scaffolding protein filamin A (FLNA) (*5*, *6*) is elevated in the cortex and olfactory bulb of conditional *Tsc1*[null] mice, in the cortex of individuals with TSC, and in cells expressing constitutively active ras homolog enriched in brain (Rheb[CA]), the canonical activator of mTOR (*7*, *8*). This increase in FLNA was independent of mTOR activity (meaning rapamycin insensitive) but dependent on mitogen-activated protein kinase (MAPK) kinase (MEK) activity (*7*). In addition, normalizing FLNA expression in olfactory bulb *Tsc1*-null neurons through genetic knockdown prevented well-conserved features of TSC and FCDII FCMs associated with seizures. However, it remains unclear whether FLNA is increased in cortical malformations in individuals with FCDII and whether it contributes to seizures in mouse models of TSC and FCDII.

We therefore examined whether FLNA expression was also increased in the cortex of individuals with epilepsy and FCM diagnosed as FCDII by magnetic resonance imaging (MRI) and post-surgery pathological examination. We found that FLNA was increased in dysmorphic cells, including Balloon cells and cytomegalic neurons, in human FCDII tissue that was surgically resected for epilepsy treatment. FCDII can result from a spectrum of mutations in phosphoinositide 3-kinase (PI3K)–Rheb pathway genes upstream of mTOR as well as gain-of-function mutations in the mTOR gene itself (*9*–*11*). Whereas we previously reported that Rheb[CA] expression increases FLNA expression in cells, additional experiments revealed that mTOR gain-of-function mutations did not increase FLNA in agreement with the rapamycin insensitivity of the FLNA increase (*7*). Using our Rheb[CA] mouse model of TSC and FCDII-like FCM associated with convulsive seizures (*12*), we examined whether normalizing FLNA function would alleviate cytoarchitectural abnormalities of FCM and seizures. We targeted FLNA using short hairpin RNA (shRNA) or treatment with PTI-125, a small molecule modulator of aberrant FLNA function, which is undergoing clinical trials for Alzheimer's disease (ClinicalTrials.gov no. NCT03748706). Both FLNA knockdown and PTI-125 treatments reduced seizure activity by >60% without affecting mTOR activity. Thus, targeting FLNA might provide an mTOR-independent therapeutic avenue in TSC and FCDII resulting from PI3K-Rheb pathway gene mutations, leading to mTOR hyperactivity.
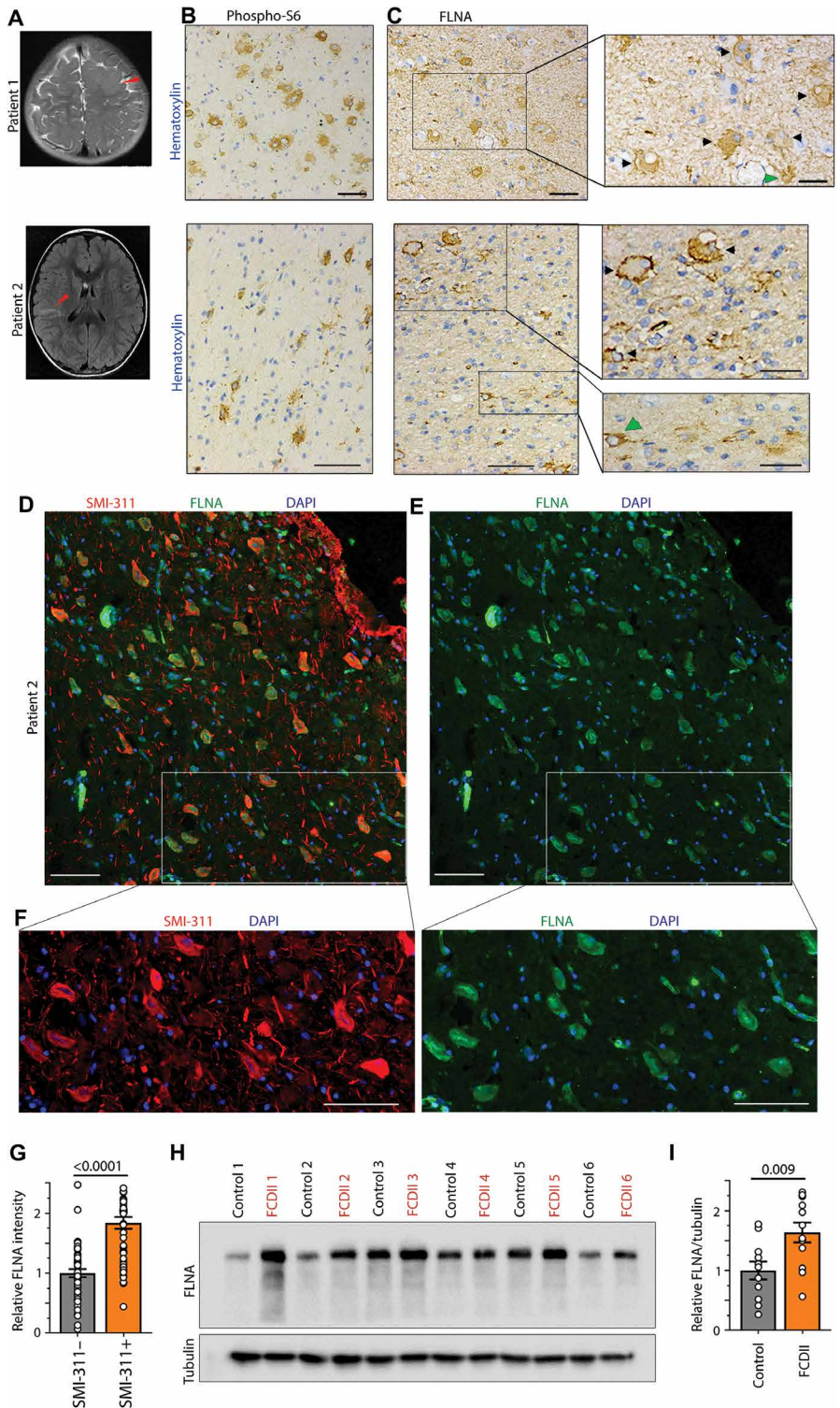
RESULTS

FLNA is increased in patients with FCDII and in Rheb[CA] mice modeling TSC and FCDII

We obtained cortical tissue samples from 17 patients with FCDII who underwent surgery for epilepsy (table S1). Every patient had FCM detected on MRI scans (two examples are shown in Fig. 1A)

[1]Departments of Neurosurgery and Cellular & Molecular Physiology, Yale University School of Medicine, New Haven, CT 06520-8082, USA. [2]Department of Neurosurgery, Xiangya Hospital, Central South University, 87 Xiangya Street, Changsha, Hunan 410008, China. [3]Cassava Sciences Inc., Austin, TX 78731, USA.
*Corresponding author. Email: angelique.bordey@yale.edu

Zhang *et al.*, *Sci. Transl. Med.* **12**, eaay0289 (2020)   19 February 2020

1 of 12

SCIENCE TRANSLATIONAL MEDICINE | RESEARCH ARTICLE

Fig. 1. FLNA expression is increased in cortices of patients with FCDII. (**A**) MRI scans of 2- and 5-year-old patients with FCDII with seizures. The red arrow points to the FCM. (**B** and **C**) Images of phospho-S6 (B) and FLNA (C) staining in hematoxylin-stained sections from the FCM in the brain of patients whose scans are shown in (A). Black and green arrows point to FLNA-positive balloon cells and dysmorphic neurons, respectively. (**D** and **E**) Coimmunostaining for FLNA and a marker of cytomegalic neurons, SMI-311, and 4′,6-diamidino-2-phenylindole (DAPI) counterstain in human FCDII tissue. (**F**) Magnification of SMI-311 or FLNA staining with DAPI from images in the white square in (D) and (E). (**G**) Quantification of FLNA staining in SMI-311–positive neurons relative to surrounding SMI-311–negative cells. Only SMI-311–negative cells with visible FLNA staining (to outline the cell body) were used for quantification. (**H** and **I**) Immunoblots of FLNA and tubulin from resected FCDII tissue (H) and quantification from 12 patients with FCDII (I). The numbers correspond to those of the patients listed in tables S1 and S2. FLNA and tubulin size were 280 and 55 kDa, respectively. Unpaired Student's t test. Data are means ± SEM. n numbers are listed in table S3. Scale bars, 100 μm.

and underwent electroencephalogram (EEG) recording with a combination of subdural grid and depth electrodes before FCM resection. All patients were identified as FCDII after surgery based on pathological examination of the hematoxylin-stained resected tissue and identification of hallmarks of FCDII, including cortical dyslamination and the presence of cytomegalic, dysmorphic neurons (table S1). The distinction between FCDIIa and FCDIIb was based on the absence or presence of balloon cells, respectively (*13*). For the FCDII tissue examined by immunohistochemistry ($n = 5$), we confirmed the presence of dysmorphic cells, including classical multinucleated balloon cells, and an increase in phosphorylated ribosomal protein S6 (phospho-S6), a readout of mTOR activity (Fig. 1B and fig. S1). These enlarged cells had increased expression of FLNA compared to surrounding normal-sized cells (Fig. 1C and fig. S1). To verify that cells expressing FLNA were neurons, we coimmunostained for FLNA and SMI-311, a marker of cytomegalic, dysmorphic neurons (*14–16*). We found that all SMI-311–positive neurons were immunoreactive for FLNA (Fig. 1, D to F, and fig. S2) and displayed significantly increased FLNA intensity compared to surrounding cells ($P < 0.0001$; Fig. 1G).

To quantify FLNA expression in patients with FCDII ($n = 12$) compared to controls, we obtained tissue from age-matched control patients who underwent surgery for brain trauma ($n = 11$; table S2) and performed immunoblotting for FLNA (Fig. 1H). As a group, FCDII tissue from 12 patients displayed significantly ($P = 0.009$) increased amount of FLNA compared to control cortical tissue (Fig. 1I and fig. S3; numbers on top of the blot correspond to patient numbers in table S1). In light of the variability of the Western blot data (ranging from 0.57 to 2.31× control values), we examined whether the amount of FLNA was correlated with the age of seizure onset, the duration of epilepsy history, and the diagnosis of FCDIIa versus FCDIIb. We found no correlation between the amount of FLNA and these parameters (fig. S4). Another parameter that may contribute to the variability in FLNA

Zhang *et al.*, *Sci. Transl. Med.* **12**, eaay0289 (2020)   19 February 2020

2 of 12

expression is the identity of the mutant genes. We previously reported that the increase in FLNA induced by *Tsc1* loss or Rheb[CA] over-expression was mTOR independent (*7*), suggesting that mutations in mTOR itself do not contribute to increases in FLNA. We tested this hypothesis in cultured neurons (14 days in vitro) nucleofected with two plasmids encoding mTOR with gain-of-function mutations reported in patients with FCDII or Rheb[CA] (*17*). The two mTOR mutations did not increase FLNA compared to control, whereas Rheb[CA] did, despite that all three conditions significantly increased phospho-S6 ($P < 0.0003$; Fig. 2, A to C, and fig. S8). Although the mutations in the human tissue used for immunoblotting were not identified, these data may explain some of the variability in the amount of FLNA in human samples. These data suggest that FLNA could be increased in patients with TSC or FCDII, resulting from PI3K-Rheb pathway gene mutations but not from mTOR mutations.

Before examining the contribution of increased FLNA to seizures, we examined whether FLNA was increased in our Rheb[CA] mouse model of TSC and FCDII-like FCM associated with seizures (*12*). This model was generated using in utero electroporation (IUE) of plasmids encoding Rheb[CA] and the fluorescent reporter green fluorescent protein (GFP) in the medial prefrontal cortex at embryonic day (E) 15 (Fig. 2D) (*12*, *18*). In control littermate mice, we expressed tdTomato instead of Rheb[CA] (*19*). The cortex of Rheb[CA]-expressing mice displayed the cytoarchitectural hallmarks of human FCM, including cell misplacement, increased soma size, and neuronal dysmorphogenesis (Fig. 3, A to D). The animals exhibited daily convulsive seizures as monitored by video-EEG at 2 to 3 months of age (movie S1 and quantified in subsequent figures). FLNA immunostaining in cortical sections of Rheb[CA]-expressing mice illustrated increased FLNA in Rheb[CA]-expressing cells (GFP[+]) compared to surrounding, non-electroporated (GFP^{−}) cells (Fig. 2, E and F). In addition, immunoblots confirmed increased FLNA in the FCM-containing cortices (ipsilateral) compared to the contralateral (non-electroporated) cortices (Fig. 2, G and H, and fig. S8).

Normalizing FLNA expression in dysmorphic neurons of mTOR-driven FCM attenuates seizure frequency

We examined whether normalizing FLNA expression would prevent some of the cytoarchitectural abnormalities found in the experimental FCM. To decrease FLNA expression in Rheb[CA]-expressing neurons, we coexpressed an shRNA against *Flna* or *luciferase* (control) using E15 IUE (*7*). We used a 1:1 ratio of FLNA shRNA to Rheb[CA] plasmid concentration because we previously reported that this ratio fully normalized FLNA expression in Rheb[CA]-containing cortical neurons in vitro (*7*). We analyzed cell placement and morphology at postnatal day (P) 28 as previously reported (*18*). *Flna* shRNA partially, but significantly, prevented neuronal misplacement (from 50 to 23% of misplaced cells versus only 2% in control, $P < 0.0001$; Fig. 3A), increased soma size (from 372 to 250% of control, $P < 0.0001$; Fig. 3B), and dendritic dysmorphogenesis (from 194 to 130% of control total dendritic length, $P < 0.0001$; Fig. 3, C and D). Considering that increased soma size is often used as a readout of increased mTOR activity and that decreasing FLNA expression reduced soma size, we examined whether *Flna* shRNA would affect the amount of phospho-S6, a more direct readout of mTOR activity than soma size. *Flna* shRNA did not prevent increased phospho-S6 intensity in vivo (see Fig. 3H). This was further confirmed in vitro in Neuro2a cells in which *Flna* shRNA did not reduce Rheb[CA]-induced increased S6 phosphorylation (fig. S5). In addition, although *Flna* shRNA reduced

Rheb[CA]-induced increase in soma size, it did not normalize it (still increased by 250%), consistent with persistent hyperactive mTOR in the *Flna* shRNA condition. Last, we obtained video-EEG recordings of Rheb[CA]-expressing mice for 5 days starting at P61 followed by pathological analysis of the tissue (Fig. 3, E and F). Mice expressing *Flna* shRNA in Rheb[CA]-expressing neurons displayed a significantly lower seizure frequency (by 83%, $P < 0.0001$) compared to mice expressing *luciferase* shRNA (mean of 2.2 versus 12.6 seizures per day; Fig. 3G). In addition, whereas 4 of 16 mice died in the control group, no mice died in the *Flna* shRNA group (out of 10 mice). Both groups of mice (*Flna* and *luciferase* shRNA) had similar increases in phospho-S6 expression (Fig. 3H). These data suggest that differences in seizure activity between the control and *Flna* shRNA condition were not due to variations in Rheb[CA]-induced mTOR activation, and thus FCM features (*20*), and that the rescue of cytoarchitectural abnormalities by *Flna* shRNA was independent of mTOR.

Long-term treatment with a small molecule modulator of FLNA, PTI-125, before seizure onset partially prevents neuronal dysmorphogenesis and reduces seizure activity

We investigated the therapeutic potential of modulating aberrant FLNA activity via a small FLNA-binding molecule, PTI-125. PTI-125 was derived from an iterative in silico/in vitro screening process against a known pentapeptide region of FLNA that was identified in an earlier study (*21*). PTI-125 has been reported to bind native FLNA as well as aberrant FLNA in Alzheimer's disease with picomolar and femtomolar affinity, respectively (*22*), and is currently in clinical trials for Alzheimer's disease (ClinicalTrials.gov no. NCT04079803). Twice-daily intraperitoneal injections of PTI-125 (salt form) (6 or 12 mg/kg) (*23*) were given to Rheb[CA]-expressing mice from P8 to P28 to test efficacy at preventing the FCM-associated cytoarchitectural abnormalities (Fig. 4A). We chose P8 because it corresponds to a newborn human, and by P28, dendritic development is complete. PTI-125 at 6 and 12 mg/kg partially rescued neuronal soma size and dendritic dysmorphogenesis, with slightly greater efficacy at a dose of 12 mg/kg (Fig. 4, B to D). We also found that phospho-S6 expression in the cortex of non-electroporated mice was not affected by PTI-125 (12 mg/kg) treatment (Fig. 4E and fig. S8). We next examined the efficacy of long-term (P8 to P65) PTI-125 treatment at 12 mg/kg on seizure activity that was recorded at P61 to P66 using video-EEG (Fig. 4F). Littermate mice were randomly split into two groups, receiving PTI-125 or saline vehicle (intraperitoneal injections, twice daily). PTI-125 treatment significantly reduced seizure frequency compared to vehicle treatment (5.1 versus 1.4 seizures per day, $P = 0.003$; Fig. 4G). This treatment did not affect body weight (Fig. 4H). In addition, cell misplacement and phospho-S6 intensity in brain sections from recorded mice were not affected by PTI-125 treatment (Fig. 4, I and J). Hence, the reduced seizure activity in PTI-125–treated mice was not due to technical issues with IUE or differences in mTOR activation between the two groups of mice. Thus, PTI-125 treatment before seizure onset efficiently reduces seizure frequency by 73% independently of mTOR.

PTI-125 after seizure onset rescues neuronal dysmorphogenesis and decreases seizure activity

We next tested whether a treatment with PTI-125 after the onset of seizures could rescue some of the morphological abnormalities and seizure activity. In our mouse model, Racine grade 4 to 5 seizures are visible by P21. A 26-day treatment with PTI-125 from P29 to P54
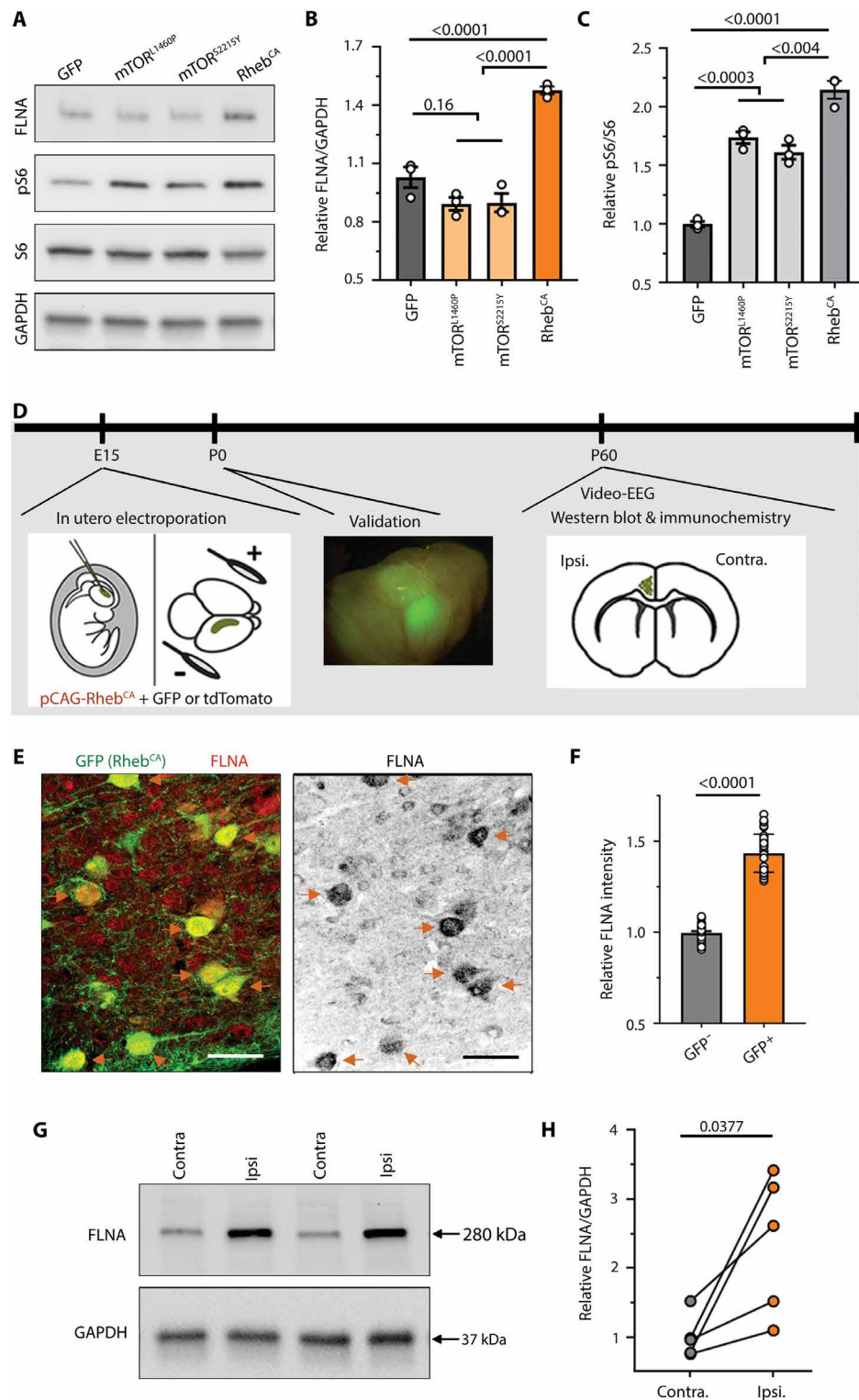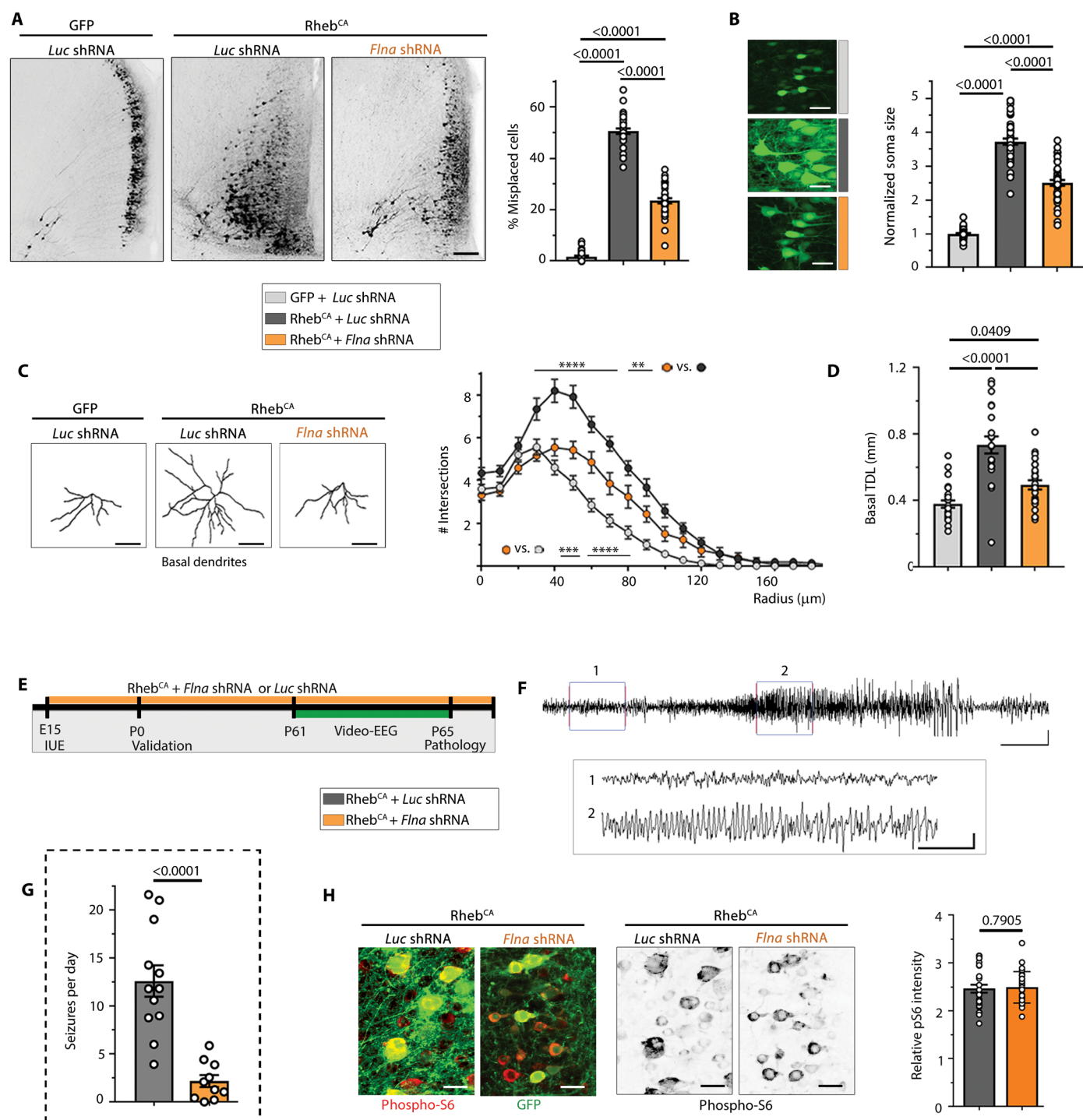
SCIENCE TRANSLATIONAL MEDICINE | RESEARCH ARTICLE

Fig. 2. FLNA expression is increased in mouse cortices containing Rheb^{CA}-induced FCM. (A) FLNA (280 kDa), phospho-S6 (pS6) (32 kDa), S6 (32 kDa), and glyceraldehyde phosphate dehydrogenase (GAPDH) (37 kDa) immunoblots in cultured neurons expressing plasmids encoding GFP, mTOR mutants, or Rheb^{CA}. **(B and C)** Quantification of the blots shown in (A). **(D)** Diagram of the experimental procedure for generating FCM in mice followed by video-EEG recordings and immunoblotting or immunochemistry. **(E and F)** FLNA immunostaining in sections from mouse FCM (E) and quantification in GFP$^+$ Rheb^{CA}-expressing cells relative to surrounding GFP$^-$ cells (F). Scale bars, 100 μm. **(G)** FLNA and GAPDH immunoblots. Ipsi, ipsilateral; Contra, contralateral. **(H)** FLNA/GAPDH quantification in FCM-containing cortices relative to contralateral cortices in mice electroporated with Rheb^{CA}. One-way ANOVA (B and C) and unpaired and paired Student's t test (F and H, respectively). Data are means ± SEM. n numbers are listed in table S3.
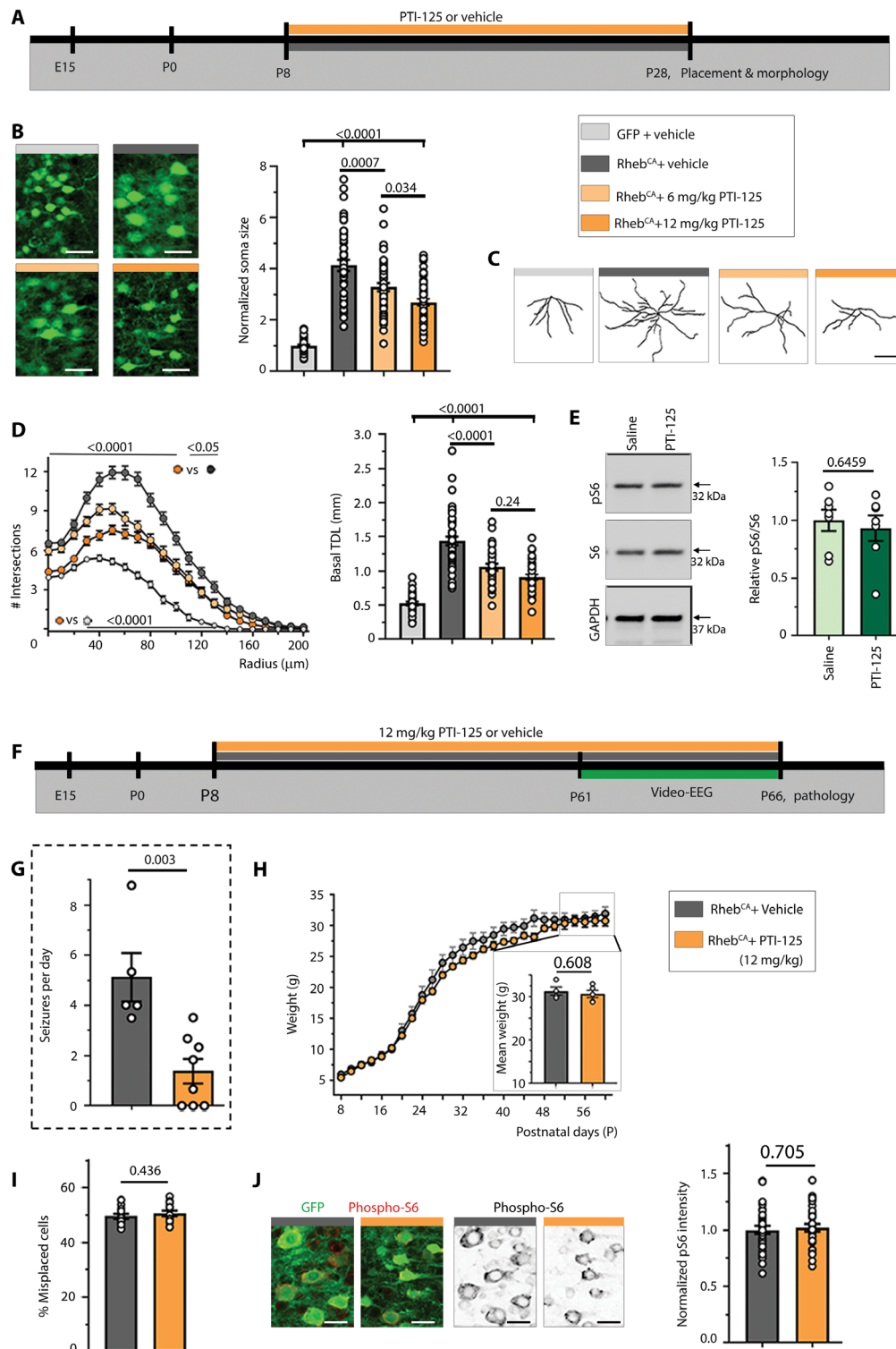
SCIENCE TRANSLATIONAL MEDICINE | RESEARCH ARTICLE

Fig. 3. Normalizing the amount of FLNA in dysmorphic neurons of mTOR-driven FCM partially prevents cytoarchitectural abnormalities and attenuates seizure activity. (**A**) Images of control or Rheb^{CA}-expressing neurons coexpressing *luciferase* or *Flna* shRNA in littermate mice, and quantification of neuronal placement in the different conditions. Scale bar, 250 μm. (**B**) Images of GFP^{+} electroporated neurons in different conditions and quantification of soma size. Scale bars, 50 μm. (**C**) Basal dendrite reconstruction and corresponding Sholl analysis. Scale bars, 50 μm. (**D**) Bar graphs of the basal total dendritic length (TDL). (**E**) Diagram of the experimental procedure. (**F**) Representative EEG traces in a control shRNA seizing mouse. Scales: 200 μV/5 s and 1 s (inset). (**G**) Frequency of seizures in the *luciferase* (*Luc*) or *Flna* shRNA condition. (**H**) Phospho-S6 immunostaining and quantification in GFP^{+} Rheb^{CA}-expressing neurons (normalized to surrounding GFP^{-} neurons) in EEG-recorded mice. Scale bars, 50 μm. Mann-Whitney tests (G), one-way ANOVA (A, B, and D) and two-way repeated-measures ANOVA (C), and Student's *t* test (H). Data are means ± SEM. *n* numbers are listed in table S3.

SCIENCE TRANSLATIONAL MEDICINE | RESEARCH ARTICLE

Fig. 4. Treatment with a small molecule modulator of FLNA, PTI-125, before seizure onset partially prevents cytoarchitectural abnormalities and reduces seizure activity. (**A**) Diagram of experimental paradigm. (**B**) Images of neuronal soma after treatment with vehicle or different PTI-125 doses and quantification. Scale bars, 50 μm. (**C** and **D**) Reconstructions of basal dendrites (C), Sholl analyses, and basal total dendritic length (D) under different treatment conditions. (**E**) Immunoblots of phospho-S6, S6, and GAPDH from the cortices of mice treated with vehicle (saline) or PTI-125, and quantification. (**F**) Diagram of experimental paradigm. (**G**) Seizure frequency (6-day-long recordings) after vehicle or PTI-125 treatment at 12 mg/kg. (**H**) Plots of the weight gain during vehicle or PTI-125 treatment from P8 to P60. Inset, mean body weight between P52 and P60. (**I**) Quantification of cell misplacement in mice treated with vehicle or PTI-125. (**J**) Images of phospho-S6 immunostaining and GFP fluorescence in coronal sections containing Rheb^{CA}-expressing cells (GFP$^+$) and corresponding phospho-S6 quantification normalized to the vehicle-treated condition. Scale bars, 50 μm. Student's *t* test (E, H, I, and J), two-way repeated-measures ANOVA (D), Mann-Whitney test (G), and one-way ANOVA (B and D). Data are means ± SEM. *n* numbers are listed in table S3.

(3-week treatment; Fig. 5A) partially, but significantly, rescued increased soma size ($P < 0.0001$; Fig. 5, B and C) and dendritic dysmorphogenesis ($P < 0.0001$; Fig. 5, D and E). To assess efficacy on seizure activity, video-EEG recordings were obtained at the end of the treatment (P50 to P54). PTI-125–treated mice displayed a significantly lower seizure frequency by 69% ($P = 0.0158$) compared to vehicle-treated mice (0.84 versus 2.7 seizures per day; Fig. 5, F and G). We then assessed the effect of PTI-125 on seizure activity in young adult (P61 to P106) mice that were recorded during saline injections and subsequently switched to PTI-125 injections to assess treatment effects in the same mice (Fig. 5H). We also recorded randomly selected littermate mice that were treated with vehicle from P61 to P92 and observed that seizure frequency increased over time (Fig. 5, I and J). In that same time frame, corresponding to a 20-day PTI-125 treatment, littermate mice that were switched from vehicle to PTI-125 after 12 days of recordings did not have the increase in seizure frequency observed in the vehicle group (Fig. 5, I and J). Moreover, extended recording of the PTI-125–treated mice showed that a 33-day treatment led to a significant 60% reduction ($P = 0.0156$) in seizure frequency (mean of 1.6 versus 3.9 seizures per day; Fig. 5K). Thus, PTI-125 treatment after the onset of seizures in either juvenile or adult mice decreased seizure frequency and prevented the worsening of seizure activity observed over time in vehicle-injected adult mice.

Last, we combined the seizure data obtained for all the PTI-125 treatments and compared them to their corresponding vehicle treatments (data from Figs. 4G, 5G, and 5K corresponding to P8 to P65, P29 to P54, and P71 to P91 treatments, respectively). PTI-125 treatments significantly increased the number of seizure-free mice (35 versus 11%, $P = 0.0343$; Fig. 6A). In addition, mice treated with PTI-125 ($n = 32$) exhibited an overall 66% reduction in seizure frequency compared to vehicle-treated littermates ($n = 27$), illustrated in a heat map (Fig. 6B) and scatter graph ($P < 0.0001$; Fig. 6C).
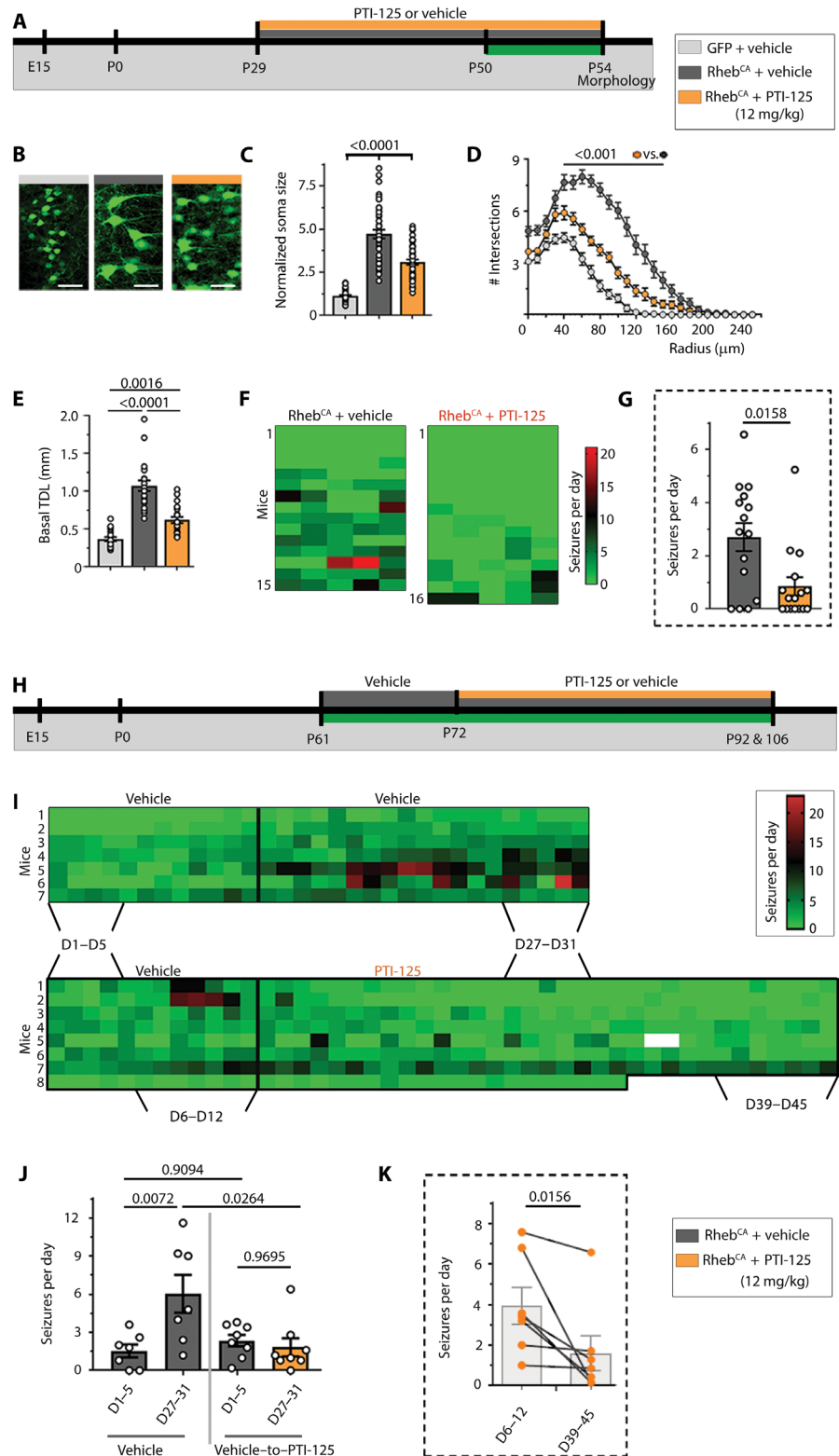
DISCUSSION
We found that cortical tissue from patients with FCDII displayed increased FLNA. In addition, the increase in FLNA was observed in SMI-311–immunopositive enlarged neurons and cells resembling balloon cells. These findings are in agreement with our previous study reporting increased FLNA expression in $Tsc1^{null}$ neurons in vivo and Rheb^{CA}-expressing cortical neurons in vitro as well as in cortical tissue from individuals with TSC (7). However, there was a marked variability in the amount of FLNA in human FCDII samples, including samples that expressed similar FLNA amount to that in controls. This variability could be explained by the fact that mutations leading to increased Rheb activity led to FLNA increases, whereas gain-of-function mutations in $mTOR$ did not. Although the genetic status of the patients was not known, it is possible that some patients had $mTOR$ mutations that would not result in increased FLNA expression. The lack of effect of hyperactive mTOR on FLNA expression is consistent with our previous observations that increased FLNA expression was due to increased transcriptional activity downstream of hyperactive MEK/MAPK independently of mTOR (7). In Rheb^{CA} mice modeling the pathology seen in TSC and FCDII, FLNA expression was also increased in Rheb^{CA} neurons and the cortex containing Rheb^{CA} neurons.

Using an shRNA against $Flna$, we found that decreasing FLNA expression in Rheb^{CA} neurons alleviated their misplacement and dysmorphogenesis, including increased soma size and dendritic complexity. The rescue of soma size was unanticipated because knocking down FLNA did not decrease mTOR activity, which is well known to regulate cell size (24). The mechanism of FLNA's role in cell size regulation is not known; FLNA could affect actin cross-linking and/or the activity of many binding partners, including previously unrecognized partners in the hyperactive mTOR condition. Identifying how knocking down FLNA alters soma size is outside the scope of the present study. Nevertheless, finding that normalizing FLNA expression did not rescue mTOR hyperactivity highlights that FLNA acts via a different mechanism than the mTOR blocker, rapamycin, to alleviate cellular abnormalities in TSC and FCDII conditions. Ultimately, normalizing FLNA expression using $Flna$ shRNA in Rheb^{CA}-expressing mice led to a decrease in seizure activity (by 83%) compared to control. This finding seems to contradict the fact that mTOR activity is required for epilepsy because rapamycin blocks seizure activity and is also sufficient for epilepsy as patients with FCDII with gain-of-function $mTOR$ mutations display seizures and expressing plasmids encoding hyperactive mutant mTOR in mice leads to seizures (9–11, 25). One possible explanation for this discrepancy is that FLNA interferes with the translation machinery downstream of mTOR, possibly through cytoskeletal reorganization [considering that polyadenylated mRNA colocalized with FLNA (26)] or its interaction with disease-specific binding partners regulating cap-dependent translation. FLNA is an actin cross-linking molecule, has multiple binding partners, and acts as a scaffolding platform inside cells where molecules can interact (5). Considering that increased soma size and dendritic tree require increased translation, a partial reduction of these defects by normalizing FLNA further suggests an interaction between FLNA and translation (18). This putative function of FLNA should be investigated in future studies. Last, although the parallel rescue of some of the morphological abnormalities and seizure activity by $Flna$ shRNA implies that these abnormalities contribute to epileptic seizures, it is possible that these rescues are coincidental, and rescuing other intracellular processes by $Flna$ shRNA may prevent seizure generation. Identifying how FLNA regulates cellular abnormalities and ultimately epilepsy, perhaps by regulating binding partners and translation, is a direction for future studies. Collectively, these data point to a critical role of FLNA in the generation of FCM and epileptic seizures.

We next examined the small molecule PTI-125, which has been reported to bind aberrant FLNA in Alzheimer's disease brain (22). Similar to $Flna$ shRNA, we found that PTI-125 ameliorated neuronal dysmorphogenesis, including increased soma size and dendritic complexity in mice treated from P8 to P28. PTI-125 treatment after P8 did not rescue neuronal placement, which is normally complete by P8. This finding suggests that the environment is not permissive for later migration and/or that once neurons have entered dendritic development (>P8), migration cannot be reinitiated. Mice treated with PTI-125, starting during the neonatal period, displayed reduced seizure frequency compared to littermate mice treated with vehicle (saline) during the same period. The fact that neuronal misplacement was not rescued, whereas seizure activity was decreased by PTI-125, is in agreement with a previous report that misplacement is not required for seizure activity (12). This finding also shows that alleviating seizure activity can be achieved even if neuronal misplacement is not rescued. Considering that most patients with epilepsy would be treated after the onset of seizures, we also examined the effects of PTI-125 on seizures after mice had experienced seizures for 1 week or for more than a month. Convulsive seizures are visible at 3 weeks of age.

Zhang *et al.*, *Sci. Transl. Med.* **12**, eaay0289 (2020)   19 February 2020

7 of 12

Fig. 5. Treatment with a small molecule modulator of FLNA, PTI-125, after seizure onset alleviates neuronal dysmorphogenesis and seizure activity. (**A**) Diagram of experimental paradigm. (**B** and **C**) Images of control GFP⁺ neurons and GFP⁺ Rheb^{CA}-expressing neurons in mice treated with vehicle (saline) or PTI-125 (B) and quantification of soma sizes (C). Scale bar, 120 μm. (**D** and **E**) Sholl analyses and basal total dendritic length. (**F**) Heat map of seizure activity over time (per day) per mouse treated with either vehicle (saline) or PTI-125. (**G**) Seizure frequency after and during vehicle or PTI-125 treatment from P29 to P54. (**H**) Diagram of experimental paradigm. (**I**) Heat map of seizure activity per individual mouse over time. In the upper heat map, mice received vehicle injections and were recorded from P61 to P92. In the bottom heat map, mice received vehicle from P61 to P72 and then PTI-125 until P106. For mouse #5, the wires were unplugged for 2 days, leading to loss of recordings that are colored white on the heat map. (**J**) Bar graph of the seizure frequency at days (D) 1 to 5 and D27 to D31 of recordings (corresponding to P61 to P65 and P88 to P92) under continuous vehicle treatment or vehicle–to–PTI-125 treatment. (**K**) Plots of the seizure frequency before and after PTI-125 treatments. One-way ANOVA (C, E, and J), two-way repeated-measures ANOVA (D), Mann-Whitney tests (G), and Wilcoxon matched-pairs test (K). Data are means ± SEM. *n* numbers are listed in table S3.

Treatment of juvenile mice with PTI-125 at P29 (about 1 week after seizure onset) partially normalized soma size and dendritic abnormalities and reduced seizure frequency (by 67%). Mice treated with PTI-125 starting at P61 (>1 month after seizure onset) and recorded before and during treatment exhibited a progressive decrease in seizure frequency over time, reaching a 60% decrease after 30 days of treatment. By contrast, seizure activity in saline-treated mice increased over time.

We acknowledge several limitations to our study. First, as mentioned above, we do not know the genetics of the patients that may lead to variability in the expression of FLNA. Second, we did not test a higher concentration of PTI-125 that may be more efficient at reducing seizure frequency. Third, we do not know the exact mode of PTI-125's action to reduce seizure activity. On the basis of mechanistic data in Alzheimer's disease mouse models and postmortem human tissue (*22*, *23*), it is possible that FLNA may have an altered conformation in the present study and thus different binding partners specific to TSC and FCDII. PTI-125 would then prevent the abnormal binding partners of FLNA, resulting in reduced TSC and FCDII pathology. This speculative mechanism and the possible abnormal binding partners would need to be investigated in future studies. It is also possible that PTI-125 reduces seizures through an FLNA-independent mechanism, perhaps by altering the excitability of the entire network, including that of normal neurons resulting in a reduction of the overall epileptogenicity of the cortex.

However, data with *Flna* shRNA indicate that normalizing FLNA expression in diseased neurons is sufficient to reduce seizure frequency, suggesting that it is PTI-125's effect on FLNA that alleviates seizures. Fourth, our seizure data are only acquired using a mouse
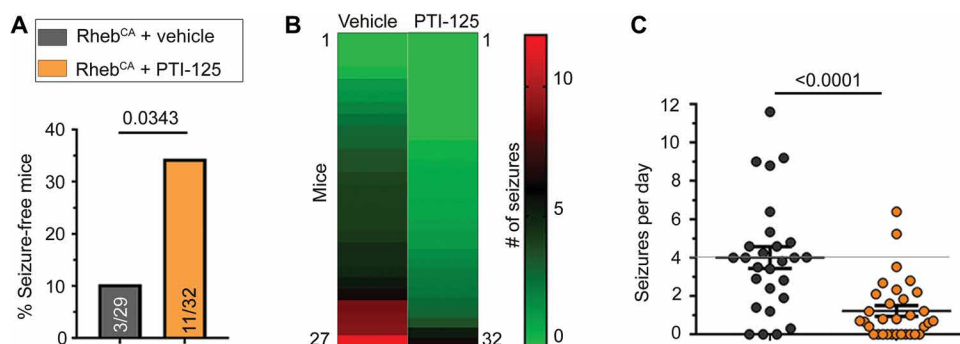
Zhang *et al.*, *Sci. Transl. Med.* **12**, eaay0289 (2020)   19 February 2020

8 of 12

SCIENCE TRANSLATIONAL MEDICINE | RESEARCH ARTICLE

Fig. 6. PTI-125 decreases the percentage of seizing mice and seizure frequency. (**A**) Percentage (%) of seizure-free mice in both conditions. Two mice in vehicle-treated condition died of seizures during EEG recordings and thus were not included in (B). (**B** and **C**) Heat map of seizure frequency for all conditions (B) and corresponding scatter plot (C). Fisher's exact test (A) and Mann-Whitney test (C). Data are means ± SEM.

model of the TSC and certain FCDII. It is unknown whether data obtained in rodents would be applicable to humans. Considering that our Rheb^CA mouse model recapitulates the pathological features of FCM observed in humans, including mislamination, white matter heterotopia, neuronal dysmorphogenesis, and hyperactive mTOR (*12, 18, 20, 27*), and the increase in FLNA is also observed in the cortices of patients with TSC and FCDII, we hope that our seizure data will be applicable to humans. Regarding PTI-125, no toxicity has been reported after phase 1 of the clinical trial for Alzheimer's disease, but it has not been tested in younger subjects. In addition, pharmacokinetic and pharmacodynamic studies would need to be performed in mice of different ages to determine whether one or multiple injections per day would be more optimal for treatment.

In conclusion, targeting FLNA with shRNA gene therapy or the small molecule PTI-125 may offer an alternative option for treating seizures and epilepsy in patients with TSC or selective FCDII without altering mTOR activity. These treatment options would likely not be applicable to all patients with FCD but those with mutations in PI3K-Rheb pathway genes. The proposed treatment would nevertheless be applicable to all TSC individuals. The findings presented here suggest the possibility of combination therapy with mTOR blocker, everolimus (a rapamycin derivate), perhaps at lower and less adverse doses. A more thorough study of dosing and duration of treatment might identify a regimen to enhance PTI-125's efficacy in treating seizures. Clinical development of PTI-125 for another indication (Alzheimer's disease) is already underway, which should greatly facilitate clinical application in patients with TSC and FCDII with mutations in PI3K-Rheb pathway genes.

MATERIALS AND METHODS
Study design
Our research objectives were to investigate whether the expression of FLNA was increased in tissue from FCDII individuals and the cortices of mice modeling FCDII and to then examine whether decreasing the amount of FLNA or its function was sufficient to reduce seizures. We have extensive experience with the mouse model that we developed. To decrease FLNA expression, we used an shRNA strategy as we previously reported (*7*). The shRNA plasmid and FLNA antibody were validated. The quantity of shRNA used was based on our previous study. To block FLNA function, we used a small molecule PTI-125. The dosage of PTI-125 was determined first by

testing the effects of PTI-125 on cell placement and morphology. The treatment paradigm was chosen to match several developmental milestones. Experimental and control animals were littermate, although several litters had to be used for most experiment, and none were excluded from analysis at the time of harvest. Experimental animals were lost before or during seizure recordings either due to sudden death by seizure or due to technical issues with the recording system. No attempt was made to segregate results based on gender or sex. Analysis was performed blindly, and seizure analysis was performed by two investigators. In addition, mice were randomly split into different groups for drug injection. Blinding was performed at multiple points during the experiments. For example, after video-EEG recording, the recording files were renamed for analysis by investigators blinded to the treatment condition.

Normality was checked with D'Agostino and Pearson normality test. Sample sizes were estimated on the basis of our previous experience for studying both the anatomy and seizure activity. The sample size calculation was performed using power analysis with G*Power 3 (*28*). For each set of experiment, the sample size was estimated for an effect size of 50% using SD calculated from the control population and a power at 80% (β = 0.2) and an α of 0.05. After experiment, for Fig. 5G, for example (effect of PTI-125 treatment from P29 to P54 on seizure frequency), using a Mann-Whitney test (two groups, non-equal SD and not normal distribution, two tails), 13 mice in each group would be sufficient to reach significance with a power of 0.9 and an α of 0.05 for the presented data. Each experiment was reproduced at least three times with $n \geq 3$, as detailed in table S3. We removed one mouse for the video-EEG data in Fig. 4G. The mouse displayed no seizure despite bilateral electroporation of Rheb^CA, and after examination of the brain sections, very few electroporated cells were found per section (<10 cells). Electroporation was thus unsuccessful. The brain of every recorded mouse was examined post-EEG recording to ensure that the mouse with no seizure had proper electroporation. Raw data are reported as separate Excel document in data file S1.

Animals
Research protocols were approved by the Yale University Institutional Animal Care and Use Committee. All experiments were performed on CD-1 mice (Charles River) of either sex.

Human tissue sample
Human tissue was obtained directly from the surgery room and rapidly frozen in liquid nitrogen and then stored at −80°C (for immunoblotting and immunostaining) or fixed in 10% formalin (for immunohistochemistry). Human tissue collection and use was approved by the human ethical committee in Xiangya Hospital, Central South University, China. Patient information is provided in tables S1 and S2. The mean age of the control patients and patients with FCDII was 13.5 ± 2.02 (*n* = 11) and 15.08 ± 2.47 years (*n* = 12), respectively.

Zhang *et al.*, *Sci. Transl. Med.* **12**, eaay0289 (2020)   19 February 2020

9 of 12

IUE and plasmids

Each DNA plasmid was diluted in sterile phosphate-buffered saline (PBS) (pH 7.4) to a final concentration listed in table S4. Timed pregnant mice (embryonic day, E15) were anesthetized with isoflurane. After exposing the uterine horns, ~1.5 μl of DNA solution, containing 0.1% fast green added as an injection tracer, was injected into the lateral ventricle via a pulled glass capillary. PBS-soaked tweezer-type electrodes (model 520, BTX) were then positioned on the head of the fetuses across the uterine wall, and six square pulses at 42-mV and 50-ms duration every 950 ms were applied using a pulse generator (ECM830, BTX). At birth, mice were prescreened for successful electroporation by detecting the expression of fluorescent protein markers on a fluorescence-enabled stereo microscope (SZX16, Olympus). Morphology and seizure data in different conditions (*Flna* versus *luciferase* shRNA or vehicle versus PTI-125 treatment) were compared between littermate mice. For most experiments, mice received unilateral electroporation, except for experiments in Fig. 3G (P8 to P65 PTI-125 treatment on seizures) for which mice received bilateral electroporation.

Transcardial perfusion and immunofluorescence
Mice

Mice were transcardially perfused with PBS followed by 4% paraformaldehyde. Brains were then dissected and postfixed in 4% paraformaldehyde for 24 hours before being transferred to a solution of 3% agarose solution in PBS. These were then sectioned coronally on a vibratome at a thickness of 50 μm. For immunofluorescence, free-floating sections were incubated for 1 hour in a blocking solution (2% bovine serum albumin and 0.1% Triton X in PBS) at room temperature and then incubated with primary antibodies (table S5) overnight at 4°C. Sections were washed with PBS + 0.05% Tween 20 and then placed in blocking solution containing secondary antibodies for 1 hour at room temperature. All images were taken using an FV1000 confocal microscope (Olympus).

Humans

For immunohistochemistry analysis, human samples were frozen in liquid nitrogen or fixed in 10% formalin and embedded in paraffin for preparing serial sections (4 μm thick) that were then deparaffinized and rehydrated by immersion in xylene followed by ethanol gradients. Slices were soaked in citrate solution followed by boiling in a microwave (for antigen unmasking) and washed in 3% hydrogen peroxide. Tissue sections were incubated with primary antibodies (table S5) overnight at 4°C in a moist chamber. After washing with PBS, slices were incubated with secondary antibody for 30 min at room temperature. Sections were mounted after dehydration.

Quantification of neuronal distribution, soma size, and staining intensity

Quantification of the number of layer 2/3 neurons in the anterior cingulate cortex, the boundary between layer 2/3, and layer 5 was determined using ER81 staining, which labels layer 5 (fig. S6). Soma size was quantified by outlining the soma of GFP$^+$ cells and measuring the area using ImageJ. Intensity of phospho-S6 and FLNA in sections was quantified by outlining somas of cells and measuring the mean gray value. Then, the values in electroporated cells (in mice) or SMI-311–positive cells (in humans) were normalized to those in non-electroporated cells or unstained cells surrounding electroporated cells to control for variability of staining between sections.

Sparse neuron electroporation and quantification of dendritic trees

To analyze neuronal morphology, and in particular dendritic trees, we labeled only a few neurons per section using a Cre-based strategy as previously reported (*29*). More specifically, we used an inducible DsRed2 vector (pCAG-LoxP-stop-LoxP-DsRed2, pCALNL-DsRed2) combined with a Cre vector (pCAG-Cre) used at a very low concentration (1 ng/μl). The Cre plasmid led to DsRed expression in only three to five neurons per slice, allowing us to cleanly analyze the dendritic morphology of individual neurons (fig. S7). Images of DsRed-expressing basal dendrites were acquired in coronal sections using a Fluoview 1000 confocal microscope with a 20× objective. Basal dendrites were traced with simple neurite tracer software (FIJI and NeuronStudio). Sholl analyses were carried out using the number of intersections in 10 μm–increment concentric circles as a measure of morphological complexity. Z stacks from three different square fields of view were taken from three different sections. Analysis was performed blindly with more than four animals and more than 20 cells per condition (see table S3 for actual *n* number).

Neuro2a cell culture and transfection

Neuro2a cells were grown at 37°C with 5% CO_2 in complete medium consisting of high-glucose Dulbecco's modified Eagle's medium (DMEM) (Gibco, no. 11965-092), 5% heat-inactivated fetal bovine serum (Gibco, no. 16140071), and 1% penicillin-streptomycin. Cells were plated in 12-well culture plates (Corning, no. 0720082) and transfected when they reached ~70% confluence. Transfection was done using PolyJet transfection reagent (Signagen, SL100688) according to the manufacturer's instructions. Cells were lysed 72 hours after transfection for all experiments.

Nucleofection and culture of E15 cortical neurons

The medial prefrontal cortexes of E15 pups were dissected out and incubated in papain digestion solution (Worthington, no. LK003176) for 15 min at 37°C. The cortexes were then transferred to plating medium (MEM supplemented with 5% fetal bovine serum, 0.45% glucose) and dissociated by using glass pipette. After dissociation, cells were nucleofected using a Mouse Neuron Nucleofector kit (Lonza, no. VPG-1001) according to the manufacturer's instructions. Cells were finally plated on poly-D-lysine–coated six-well plates (BD Biosciences, no. 354413). The medium was changed to neuronal maintenance medium (neurobasal with 1× B27 and 1× GlutaMAX-1) 2 hours after plating. Protein extraction and Western blots were performed 14 days after nucleofection.

Western blot

Human and mouse samples were lysed in radioimmunoprecipitation assay buffer (Thermo Fisher Scientific, no. 89900) with protease/phosphatase inhibitor cocktail (Cell Signaling Technology, no. 5872), 5 mM EDTA, and deoxyribonuclease I (20 units/ml; Roche). All lysates were run on tris-glycine gels (Bio-Rad, no. 456-1086 for mouse samples and no. 456-1046 for human samples). Proteins were transferred to polyvinylidene difluoride and blocked in 5% milk and incubated with primary antibodies (concentrations of primary antibody are listed in table S5). Horseradish peroxidase–conjugated anti-rabbit or anti-mouse was used as secondary antibodies. Phosphorylated and total proteins were blotted on the same membrane after stripping (Thermo Fisher Scientific, no. 21059). All density measurements were performed using National Institutes of Health

Zhang *et al.*, *Sci. Transl. Med.* **12**, eaay0289 (2020)   19 February 2020

10 of 12

(NIH) ImageJ software. In the case where cross-blot normalization was required, a reference sample was loaded on each gel to account for intergel variability (fig. S3).

EEG headmount implantation

Prefabricated EEG headmounts (Pinnacle Technology, catalog no. 8201-EEG) were implanted in 6- to 8-week-old mice. Mice were anesthetized with isoflurane and positioned on a stereotaxic frame using ear bars. A rostro-caudal midline incision was made in the skin to expose the skull surface. Four pilot holes (two bilateral holes 1 mm anterior to bregma and two bilateral holes 5 mm posterior to bregma, each 1.5 mm lateral to sagittal suture) was tapped through the skull to dura using a microdrill (Roboz Surgical Instrument, no. RS6300). The headmount was attached on top of the skull by threading four stainless steel screws (Pinnacle Technology, catalog no. 8209) into the pilot holes. Silver conductive paint (Electron Microscopy Sciences) was applied around the screw threads to ensure a solid connection with the headmount. The entire implant was insulated using dental acrylic. Mice were allowed to recover in their home cage for 7 days before video-EEG monitoring.

Video-EEG recordings and analysis

Mice were housed in individual recording chambers in a light-, temperature-, and humidity-controlled room during video-EEG monitoring. Mice were freely moving inside the chambers and had ad libitum access to food and water. Synchronous video-EEG recording was acquired using a three-channel EEG tethered system (Pinnacle Technology, catalog no. 8200-K1-iSE3) and Sirenia Acquisition software (Pinnacle Technology). Mice were continuously recorded 24 hours/day for 5 to 6 consecutive days or 31 to 45 days.

Seizure frequency and duration were analyzed using Sirenia Seizure Basic software (Pinnacle Technology). All analyses were performed blinded to experimental groups by at least two investigators. The entire EEG traces were manually reviewed for the occurrence of seizures, defined as a sudden onset of high-amplitude activity with a characteristic pattern of progressive frequency and amplitude changes over the course of the event lasting $\geq$10 s. Seizure onset was defined by high-amplitude firing >2× baseline, and seizure termination was defined by a return to baseline activity. Video data were inspected for behavioral correlates including myoclonic jerks, tonic-clonic activities, convulsions, and loss of postural control (rearing and falling) and were used as secondary verification of seizures. For each individual animal, mean number of seizures per day was obtained by dividing the total number of seizures by the total number of recording hours and multiplied by 24.

Drug injections

PTI-125 was dissolved in saline at a concentration of 2.4 mg/ml. Mice received two intraperitoneal injections of PTI-125 (6 or 12 mg/kg) every day. Saline was used as vehicle treatment.

Statistical analyses

All analyses were conducted blindly, knowing only the arbitrarily assigned animal ID (independent of electroporation condition). Statistical tests and plots were performed using Prism 7 (GraphPad Software Inc.). Statistical significance was determined using Student's t test (two-tailed, paired or unpaired), one-way analysis of variance (ANOVA), two-way ANOVA (repeated measures, with Sidak or Tukey multiple comparisons posttest), Wilcoxon matched-pairs signed-rank test, Mann-Whitney U test (two-tailed), and Fisher's exact test, with $P < 0.05$ for significance for all experiments. Data are presented as means ± SEM. Table S3 details the statistical test used for each dataset as well as the n.

SUPPLEMENTARY MATERIALS

stm.sciencemag.org/cgi/content/full/12/531/eaay0289/DC1
Fig. S1. FLNA expression is increased in cortices of patients with FCDII.
Fig. S2. FLNA expression is increased in cytomegalic cortical neurons of patients with FCDII.
Fig. S3. Original immunoblots for FLNA in human FCDII samples.
Fig. S4. The quantity of FLNA is not correlated to the type of FCDII or age of seizure onset or epilepsy duration.
Fig. S5. Knocking down FLNA does not affect the degree of S6 phosphorylation.
Fig. S6. Delineation of layer 2/3 and layer 5 neurons using ER81 immunostaining.
Fig. S7. Single-cell labeling for dendrite (Sholl) analysis.
Fig. S8. Original immunoblots.
Table S1. Information for patients with FCDII.
Table S2. Information for control patients.
Table S3. Summary of statistical tests.
Table S4. Plasmids.
Table S5. Primary and secondary antibodies.
Movie S1. A Racine grade 4 to 5 seizure in a Rheb^CA-expressing mouse.
Data file S1. Individual-level data for Figs. 1 to 6 and figs. S1, S4, and S5 (provided as separate Excel file).

View/request a protocol for this paper from *Bio-protocol*.

REFERENCES AND NOTES

1. P. B. Crino, mTOR signaling in epilepsy: Insights from malformations of cortical development. *Cold Spring Harb. Perspect. Med.* **5**, a022442 (2015).
2. M. Wong, Mammalian target of rapamycin (mTOR) activation in focal cortical dysplasia and related focal cortical malformations. *Exp. Neurol.* **244**, 22–26 (2013).
3. R. J. Leventer, R. Guerrini, W. B. Dobyns, Malformations of cortical development and epilepsy. *Dialogues Clin. Neurosci.* **10**, 47–62 (2008).
4. J. A. French, J. A. Lawson, Z. Yapici, H. Ikeda, T. Polster, R. Nabbout, P. Curatolo, P. J. de Vries, D. J. Dlugos, N. Berkowitz, M. Voi, S. Peyrard, D. Pelov, D. N. Franz, Adjunctive everolimus therapy for treatment-resistant focal-onset seizures associated with tuberous sclerosis (EXIST-3): A phase 3, randomised, double-blind, placebo-controlled study. *Lancet* **388**, 2153–2163 (2016).
5. F. Nakamura, T. P. Stossel, J. H. Hartwig, The filamins: Organizers of cell structure and function. *Cell Adh. Migr.* **5**, 160–169 (2011).
6. Y. Feng, C. A. Walsh, The many faces of filamin: A versatile molecular scaffold for cell motility and signalling. *Nat. Cell Biol.* **6**, 1034–1038 (2004).
7. L. Zhang, C. M. Bartley, X. Gong, L. S. Hsieh, T. V. Lin, D. M. Feliciano, A. Bordey, MEK-ERK1/2-dependent FLNA overexpression promotes abnormal dendritic patterning in tuberous sclerosis independent of mTOR. *Neuron* **84**, 78–91 (2014).
8. L. Zhang, T. Huang, A. Bordey, *Tsc1* haploinsufficiency is sufficient to increase dendritic patterning and Filamin A levels. *Neurosci. Lett.* **629**, 15–18 (2016).
9. E. Marsan, S. Baulac, Review: Mechanistic target of rapamycin (mTOR) pathway, focal cortical dysplasia and epilepsy. *Neuropathol. Appl. Neurobiol.* **44**, 6–17 (2018).
10. V. Salinas, P. Vega, M. V. Piccirilli, C. Chicco, C. Ciraolo, S. Christiansen, D. Consalvo, J. Perez-Maturo, N. Medina, D. Gonzalez-Moron, V. Novaro, C. Perrone, M. D. C. Garcia, G. Agosta, W. Silva, M. Kauffman, Identification of a somatic mutation in the RHEB gene through high depth and ultra-high depth next generation sequencing in a patient with Hemimegalencephaly and drug resistant Epilepsy. *Eur. J. Med. Genet.* **62**, 103571 (2018).
11. S. Zhao, Z. Li, M. Zhang, L. Zhang, H. Zheng, J. Ning, Y. Wang, F. Wang, X. Zhang, H. Gan, Y. Wang, X. Zhang, H. Luo, G. Bu, H. Xu, Y. Yao, Y.-w. Zhang, A brain somatic *RHEB* doublet mutation causes focal cortical dysplasia type II. *Exp. Mol. Med.* **51**, 84 (2019).
12. L. S. Hsieh, J. H. Wen, K. Claycomb, Y. Huang, F. A. Harrsch, J. R. Naegele, F. Hyder, G. F. Buchanan, A. Bordey, Convulsive seizures from experimental focal cortical dysplasia occur independently of cell misplacement. *Nat. Commun.* **7**, 11753 (2016).
13. I. Blümcke, M. Thom, E. Aronica, D. D. Armstrong, H. V. Vinters, A. Palmini, T. S. Jacques, G. Avanzini, A. J. Barkovich, G. Battaglia, A. Becker, C. Cepeda, F. Cendes, N. Colombo, P. Crino, J. H. Cross, O. Delalande, F. Dubeau, J. Duncan, R. Guerrini, P. Kahane, G. Mathern, I. Najm, C. Ozkara, C. Raybaud, A. Represa, S. N. Roper, N. Salamon, A. Schulze-Bonhage, L. Tassi, A. Vezzani, R. Spreafico, The clinicopathologic spectrum of focal cortical dysplasias: A consensus classification proposed by an ad hoc Task Force of the ILAE Diagnostic Methods Commission. *Epilepsia* **52**, 158–174 (2011).
14. D. Lurton, E. M. Yacubian, E. G. Sanabria, A. Valotta da Silva, R. Vianna, E. Garzon, A. Sakamoto, R. Spreafico, E. A. Cavalheiro, Immunohistochemical study of six cases

of Taylor's type focal cortical dysplasia: Correlation with electroclinical data. *Epilepsia* **43** (suppl. 5), 217–219 (2002).

15. A. Finardi, F. Colciaghi, L. Castana, D. Locatelli, C. E. Marras, P. Nobili, M. Fratelli, M. A. Bramerio, G. Lorusso, G. S. Battaglia, Long-duration epilepsy affects cell morphology and glutamatergic synapses in type IIB focal cortical dysplasia. *Acta Neuropathol.* **126**, 219–235 (2013).

16. R. Spreafico, G. Battaglia, P. Arcelli, F. Andermann, F. Dubeau, A. Palmini, A. Olivier, J. G. Villemure, D. Tampieri, G. Avanzini, M. Avoli, Cortical dysplasia: An immunocytochemical study of three patients. *Neurology* **50**, 27–36 (1998).

17. A. M. D'Gama, M. B. Woodworth, A. A. Hossain, S. Bizzotto, N. E. Hatem, C. M. LaCoursiere, I. Najm, Z. Ying, E. Yang, A. J. Barkovich, D. J. Kwiatkowski, H. V. Vinters, J. R. Madsen, G. W. Mathern, I. Blümcke, A. Poduri, C. A. Walsh, Somatic mutations activating the mTOR pathway in dorsal telencephalic progenitors cause a continuum of cortical dysplasias. *Cell Rep.* **21**, 3754–3766 (2017).

18. T. V. Lin, L. Hsieh, T. Kimura, T. J. Malone, A. Bordey, Normalizing translation through 4E-BP prevents mTOR-driven cortical mislamination and ameliorates aberrant neuron integration. *Proc. Natl. Acad. Sci. U.S.A.* **113**, 11330–11335 (2016).

19. M. Pathania, J. Torres-Reveron, L. Yan, T. Kimura, T. V. Lin, V. Gordon, Z.-Q. Teng, X. Zhao, T. A. Fulga, D. Van Vactor, A. Bordey, miR-132 enhances dendritic morphogenesis, spine density, synaptic integration, and survival of newborn olfactory bulb neurons. *PLOS ONE* **7**, e38174 (2012).

20. L. H. Nguyen, T. Mahadeo, A. Bordey, mTOR hyperactivity levels influence the severity of epilepsy and associated neuropathology in an experimental model of tuberous sclerosis complex and focal cortical dysplasia. *J. Neurosci.* **39**, 2762–2773 (2019).

21. L. H. Burns, H.-Y. Wang, PTI-609: A novel analgesic that binds filamin A to control opioid signaling. *Recent Pat. CNS Drug Discov.* **5**, 210–220 (2010).

22. H. Y. Wang, K. C. Lee, Z. Pei, A. Khan, K. Bakshi, L. H. Burns, PTI-125 binds and reverses an altered conformation of filamin A to reduce Alzheimer's disease pathogenesis. *Neurobiol. Aging* **55**, 99–114 (2017).

23. H.-Y. Wang, K. Bakshi, M. Frankfurt, A. Stucky, M. Goberdhan, S. M. Shah, L. H. Burns, Reducing amyloid-related Alzheimer's disease pathogenesis by a small molecule targeting filamin A. *J. Neurosci.* **32**, 9773–9784 (2012).

24. A. Biever, E. Valjent, E. Puighermanal, Ribosomal protein S6 phosphorylation in the nervous system: From regulation to function. *Front. Mol. Neurosci.* **8**, 75 (2015).

25. J. S. Lim, W.-i. Kim, H.-C. Kang, S. H. Kim, A. H. Park, E. K. Park, Y.-W. Cho, S. Kim, H. M. Kim, J. A. Kim, J. Kim, H. Rhee, S.-G. Kang, H. D. Kim, D. Kim, D.-S. Kim, J. H. Lee, Brain somatic mutations in MTOR cause focal cortical dysplasia type II leading to intractable epilepsy. *Nat. Med.* **21**, 395–400 (2015).

26. G. J. Bassell, C. M. Powers, K. L. Taneja, R. H. Singer, Single mRNAs visualized by ultrastructural in situ hybridization are principally localized at actin filament intersections in fibroblasts. *J. Cell Biol.* **126**, 863–876 (1994).

27. X. Gong, L. Zhang, T. Huang, T. V. Lin, L. Miyares, J. Wen, L. Hsieh, A. Bordey, Activating the translational repressor 4E-BP or reducing S6K-GSK3β activity prevents accelerated axon growth induced by hyperactive mTOR in vivo. *Hum. Mol. Genet.* **24**, 5746–5758 (2015).

28. F. Faul, E. Erdfelder, A.-G. Lang, A. Buchner, G*Power 3: A flexible statistical power analysis program for the social, behavioral, and biomedical sciences. *Behav. Res. Methods* **39**, 175–191 (2007).

29. O. S. Dhande, E. W. Hua, E. Guh, J. Yeh, S. Bhatt, Y. Zhang, E. S. Ruthazer, M. B. Feller, M. C. Crair, Development of single retinofugal axon arbors in normal and β2 knock-out mice. *J. Neurosci.* **31**, 3384–3399 (2011).

Zhang *et al.*, *Sci. Transl. Med.* **12**, eaay0289 (2020)   19 February 2020

12 of 12

Science Translational Medicine

Filamin A inhibition reduces seizure activity in a mouse model of focal cortical malformations

Longbo Zhang, Tianxiang Huang, Shannon Teaw, Lena H. Nguyen, Lawrence S. Hsieh, Xuan Gong, Lindsay H. Burns, and Anglique Bordey

Targeting actin-binding protein in cortical malformations

Mutations in the mammalian target of rapamycin (mTOR) pathway cause focal cortical dysplasia (FCD) and tuberous sclerosis complex (TSC). These disorders are associated with pharmacoresistant epilepsy. Often, the only available treatment is the resection of the epileptic focus, an invasive intervention with severe side effects. Now, Zhang *et al.* used human brain tissue from resections and mouse models to identify pharmacological targets. They found that filamin A (FLNA) expression is increased in tissue from patients with FCD. Inhibiting FLNA in a mouse model of FCD and TSC after seizure onset reduced seizure frequency and neuronal abnormalities. The results suggest that inhibiting FLNA might be therapeutic in patients with FCD and TSC.

View the article online
https://www.science.org/doi/10.1126/scitranslmed.aay0289
Permissions
https://www.science.org/help/reprints-and-permissions

Use of this article is subject to the Terms of service